This document is the accepted version of a published work that appeared in final form in Nanomedicine, after technical editing by the publisher. To access the final edited and published work, see https://doi.org/10.1016/j.nano.2018.02.002

***Graphical Abstract: Text**

Graphical abstract - text

Folate-functionalized octahedral DNA nanocages, loaded with doxorubicin (Dox) (Dox-loaded cage), deliver the drug selectively to cancer cells expressing the α isoform of the folate receptor (αFR). Dox, released from loaded DNA cages inside cells, induces a cytotoxic effect higher than free Dox administered at the same concentration and leads to intracellular DNA nanocage degradation, avoiding the problem of nanocarrier accumulation *in vivo*.

*Graphical Abstract: Image

Click here to download high resolution image

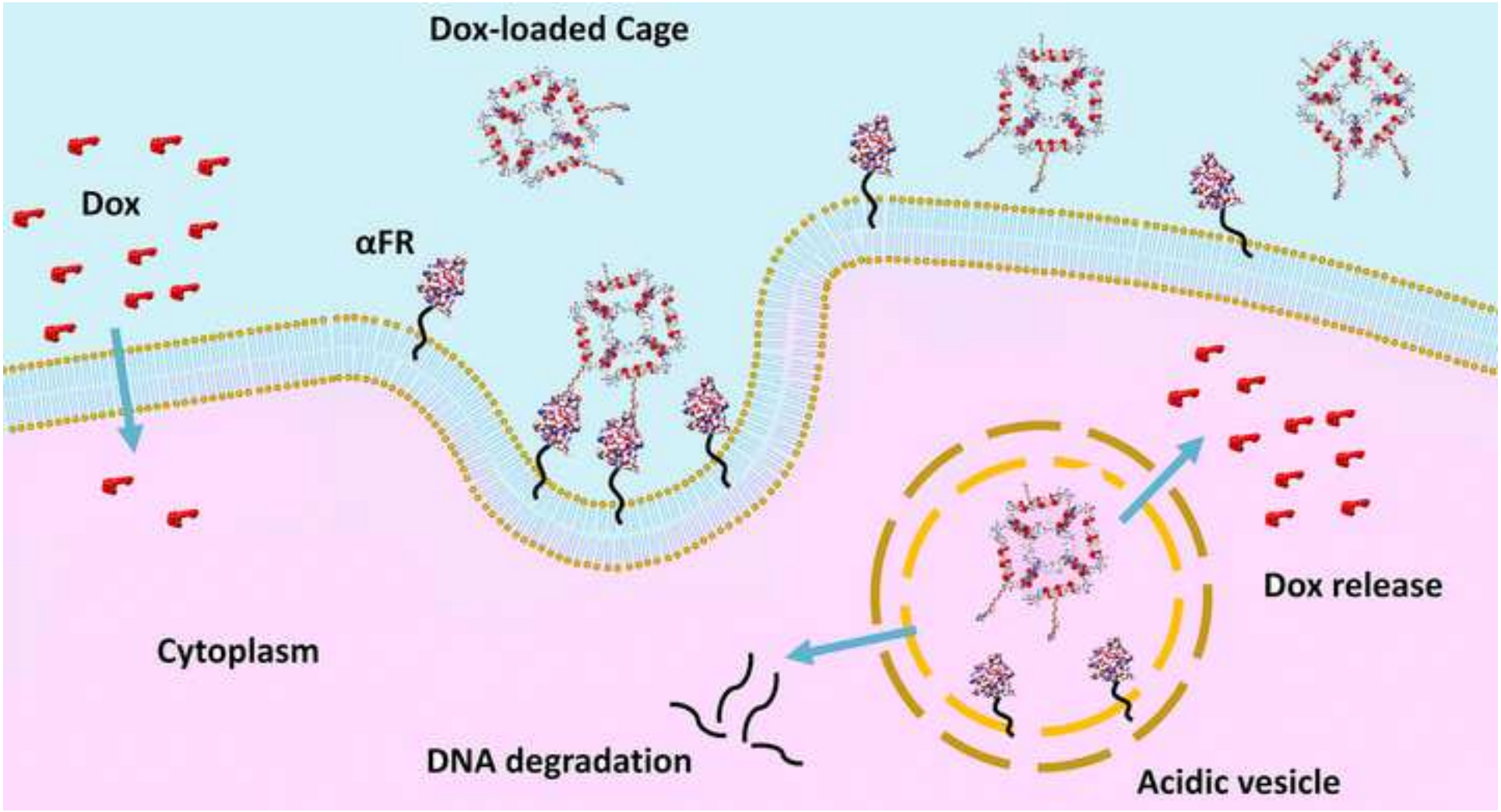

*Revised Manuscript
Click here to download Revised Manuscript: Raniolo et al second revision.docx

Selective targeting and degradation of doxorubicin-loaded folate-functionalized DNA nanocages

Sofia Raniolo[a1], MS, Giulia Vindigni[a1], PhD, Alessio Ottaviani[b], PhD, Valeria Unida[b], MS, Federico Iacovelli[b], PhD, Antonio Manetto[c], PhD, Mariangela Figini[d], MD, Lorenzo Stella[e], PhD, Alessandro Desideri[b*], PhD, Silvia Biocca[a*], PhD

[a]Department of Systems Medicine, University of Rome Tor Vergata, Via Montpellier 1, 00133, Rome, Italy.

[b]Department of Biology, University of Rome Tor Vergata, Via della Ricerca Scientifica 1, 00133, Rome, Italy.

[c] Metabion GmbH, Semmelweisstraße 3, 82152 Planegg, Germany.

[d] Department of Experimental Oncology and Molecular Medicine, Fondazione IRCCS Istituto Nazionale dei Tumori, Via Amadeo, 42 20133 Milano, Italy

[e] Department of Chemical Sciences and Technologies University of Rome Tor Vergata, Via della Ricerca Scientifica 1, 00133, Rome, Italy

Conflicts of interest: The authors declare no conflicts of interest in this work.

Financial Support Information: Research reported was supported by AIRC IG2016 (19171) and PRIN2015 (20157WW5EH) to LS.

[*]*Correspondence to:* Silvia Biocca – biocca@med.uniroma2.it; Alessandro Desideri – desideri@uniroma2.it

[1] These two authors contributed equally

Word count for Abstract: 149
Word count for manuscript: 4996
Number of References: 55
Number of figures: 7
Number of tables: 0
Number of Supplementary online-only files: 1

Abstract

Selective targeting is a crucial property of nanocarriers used for drug delivery in cancer therapy. We generated biotinylated octahedral DNA nanocages functionalized with folic acid through bio-orthogonal conjugation chemistry. Molecular modelling indicated that a distance of about 2.5 nm between folic acid and DNA nanocage avoids steric hindrance with the folate receptor. HeLa cells, a folate receptor positive tumour cell line, internalize folate-DNA nanocages with efficiency greater than 40 times compared to cells not expressing the folate receptors. Functionalized DNA nanocages are highly stable, not cytotoxic and can be efficiently loaded with the chemotherapeutic agent doxorubicin. After entry into cells, doxorubicin-loaded nanoparticles are confined in vesicular structures, indicating that DNA nanocages traffic through the endocytic pathway. Doxorubicin release from loaded DNA cages, facilitated by low pH of endocytic vesicles, induces toxic pathways that, besides selectively killing folate receptor-positive cancer cells, lead to cage degradation avoiding nanoparticles accumulation inside cells.

Keywords: DNA nanotechnology; folate-functionalized nanostructure; doxorubicin; drug delivery; selective targeting.

Introduction

The development of specialized nanoparticles is leading to novel strategies for drug delivery. Among the variety of polymers used as drug carriers, DNA emerged as one of the most suitable for the design of nanostructures, for its intrinsic properties of biocompatibility, versatility and for its unique control over nanoscale geometry and biochemical functionalization.[1] DNA strands have been used to build nanostructures with different geometry and size that can carry proteins or other functional molecules covalently attached or entrapped.[2,3,4] During the last years our group has *in vitro* and *in silico* characterized various types of fully covalently bound truncated octahedral DNA nanocages and studied their behaviour in cells.[5-10] DNA nanocages, including octahedral cages, possess many attractive properties for cancer nanotherapy: they are intrinsically nontoxic, with

excellent biocompatibility and biodegradability,[11-13] are readily internalized by living cells *via* endocytosis, [10,14] show high resistance to degradation [15,16] and can efficiently intercalate anticancer drugs such as doxorubicin.[17-20]

Doxorubicin (Dox) is one of the most commonly used anticancer agents for the treatment of a wide variety of solid tumours including breast, ovarian, prostate, brain, cervix and lung cancers and haematological malignancies, such as multiple myeloma, several types of leukaemia and lymphomas.[21] Dox has multiple mechanisms of action, including the intercalation between base pairs of the DNA helix, preventing DNA replication, disruption of topoisomerase-II-mediated DNA repair and generation of reactive oxygen species.[22,23] These different effects culminate in either cell death or cell growth arrest, through various cell biological events, such as apoptosis, autophagy, senescence and necrosis.[24,25] One of the key problems in delivering Dox to cancer cells is its lack of selectivity, which forces high dose administration, with consequent debilitating side effects. Among the tumour-associated antigens, the alpha isoform of the folate receptor (αFR) is a good target molecule. αFR, a glycosylphosphatidylinositol (GPI) membrane protein, is over-expressed in many malignant tumours of epithelial origin and is largely absent in normal tissues.[26] Its expression is not altered after chemotherapy,[27,28] making it a potential target even in treated relapsing tumours. αFR binds folic acid with a dissociation constant (K_d) of 10^{-10} M and conjugation of folate with different types of molecules, including nanoparticles, does not alter the high affinity for its receptor.[29-32] Many αFR-targeting approaches, including folic acid derivatives, folate-drug-conjugates and monoclonal antibodies, have been developed for clinical application for both imaging and therapeutic purposes.[33] Folate-conjugation has also been applied to DNA nanotubes [34,35] or DNA tetrahedral nanoparticles[36] and resulted in successful targeting to αFR overexpressing cancer cells. Here we generated biotinylated octahedral DNA nanocages functionalized with folic acid through bio-orthogonal conjugation chemistry. DNA nanocages were loaded with doxorubicin, exploiting the DNA-intercalating properties of this molecule, for treatment of cancer cells. The selective delivery, internalization, degradation and cytotoxic efficacy of Dox-loaded nanocages were analysed. Efficient uptake of the octahedral cages into cells was observed only in αFR expressing cells, demonstrating a folate receptor-mediated uptake mechanism. The high targeting efficiency translated into a selective death of αFR expressing cancer cells and degradation of nanocages.

Methods

Preparation of biotin and folate decorated DNA structures

Biotinylated DNA octahedral cages were prepared as described.[10] Oligonucleotide sequences are reported in Supplementary Material, Table S1. A folate-modified oligonucleotide was prepared starting from a double alkyne-modified oligonucleotide generated by solid-phase synthesis (Supplementary Material, S2). The C8-Alkyne-dU phosphoramidite was selected as alkyne source due to the C8-linker, which points out the helix major groove ensuring high labelling yields.[37] The post-synthesis conjugation with folate-PEG3-azide (Baseclick GmbH, Neuried, Germany) was afforded by a copper-mediated azide/alkyne cycloadditon (CuAAC, click reaction) using the OligoClick-Kit from Baseclick following the manufacturer instructions. All oligonucleotides were HPLC purified and purchased from IDT (Integrated DNA Technology, Leuven, Belgium) with the exception of the biotinylated oligo (OL2BIO Baseclick), which was obtained from Baseclick.

Modelling of the nanocage-folate receptor interaction and analysis of the electrostatic potential distribution

The truncated octahedral cage 3D model was obtained through the Polygen suite,[8] the crystal structure of the folate receptor alpha-folic acid bimolecular complex was downloaded from the PDB database with ID: 4LRH.[38] Biotin and folic acid structures were obtained from the PubChem database.[39] Spacers linking biotin or folate to thymidine were modelled using the MarvinSketch program (https://www.chemaxon.com/products/marvin/), an advanced chemical editor for drawing chemical structures. The dT-spacer-biotin and dT-spacer-folate were conjugated to the cage structure using Tripos Sybyl 6.0 (www.certara.com) and the resulting complex was minimized trough the ANNEAL module to remove any unfavourable interaction. The folate receptor was manually added to the biotin-folate decorated (Bio-Fol) DNA cage using, as a template, the folate molecule present within the crystal structure of the receptor.[39] A local energy minimization with the ANNEAL module, followed by a global energy minimization through the MAXIMIN module was performed to remove clashes introduced by the modelling procedure. The model was saved and exported in the PDB file format. The PDB file was converted in the PQR format to perform the electrostatic potential calculations, through the PDB2PQR program.[40] The electrostatic potential distribution was calculated at 0.5 kT/e (where k is the Boltzmann constant, T=298K and 1kT/e=0.0257 V), by solving the Poisson-Boltzmann equation through the Adaptive Poisson-Boltzmann Solver (APBS) algorithm,[41] as implemented in the PyMOL APBS Tools Plugin (https://pymolwiki.org/index.php/APBS). Pictures were produced with the PyMOL 1.8 version

molecular visualization program (The PyMOL Molecular Graphics System, Version 1.8 Schrödinger, LLC).

Cell cultures

HeLa, derived from human cervix cancer, HT29, derived from human colorectal adenocarcinoma, A431 cells derived from a human epidermoid carcinoma and COS cells, a monkey kidney fibroblast-like cell line were grown in DMEM (Dulbecco's modified Eagle's medium) (Biowest, Miami, FL) supplemented with 10% fetal bovine serum (FBS) (Gibco, Paisley, UK), L-glutamine 1mM (Sigma Aldrich, St. Louis, MO), sodium pyruvate 1mM (Biowest, Miami, FL) and 100U/ml penicillin-streptomycin (Euroclone, Devon, UK). For DNA cage experiments, cell culture medium was replaced with folate-free RPMI 1640 supplemented with 10% FBS the day before and experiments were performed in complete folate-free RPMI 1640 medium.

Purification and blotting of DNA nanocages

Cells were plated in 48 well plates at a density of $5x10^4$ cells/well and grown 24 hours in folate-free RPMI 1640 supplemented with 10% FBS. Cells were incubated with Bio-Fol DNA cages at different concentration and time (as indicated in each experiment). After incubation, cells were lysed, centrifuged, digested with proteinase K and analysed by DNA blot, as previously described.[10] Biotin detection was carried out using streptavidin-HRP (Horseradish Peroxidase) (Abcam) and visualized by enhanced chemiluminescence (ECL Plus, Euroclone). For image processing and densitometric analyses, photographic films were digitized by scanning. Bands were analysed with ImageJ software.

DNA nanocages were purified from conditioned medium after incubation with cells for different times at 37 °C. Conditioned medium was collected from each well, cleared from cellular debris by centrifugation at 10.000 rpm for 15 min and analysed by DNA blot.[10] For the preparation of DNA nanocage input samples, cages added to cell culture medium were immediately digested with proteinase K (100 µg/ml) for 1 h at 37 °C and protein digestion was stopped by adding phenylmethylsulfonyl fluoride (PMSF) to a final concentration of 5 mM.

Dox intercalation and release from DNA nanocages

Dox (Sigma) was diluted in TBS (Tris-HCl 50 mM, NaCl 150 mM, pH 7.4) at a concentration of 100 µM. DNA nanocages were incubated overnight at room temperature (RT) with Dox at 1:2 Dox:base-pairs (bp) ratio in a total reaction volume of 100 µl TBS. The unloaded Dox was removed by gel filtration through Sephadex G-25 Medium (Amersham), using Mobicol spin columns (MoBiTec GmbH). Fluorescence of free Dox in solution was measured using a Fluoromax4 single photon counting fluorimeter (Horiba) (Excitation: 485 nm; Emission: 590 nm). Dox intercalates into DNA with a consequent quenching of its intrinsic fluorescence signal.[42] The total amount of intercalated Dox was calculated from the fluorescence intensity of the sample after acidification at pH 2, which causes total Dox release from DNA and compared with a calibration curve obtained from measurements on free Dox samples at known concentration.

The percentage of Dox release is calculated from the following equation:

$$\frac{(Dox_{released} - Dox_{Ctrl})}{(Dox_{Tot} - Dox_{Ctrl})} \, x \, 100$$

Dox_{Ctrl} is the fluorescence intensity (λ=590 nm) of the sample at the starting point in TBS pH 7.4;

$Dox_{released}$ is the fluorescence intensity of the sample at each experimental point;

Dox_{Tot} is the fluorescence intensity of the sample after acidification at pH 2, which causes total Dox release from DNA nanocages.

Confocal analysis

A431 and HeLa cells were treated with empty, Dox-loaded Bio-Fol DNA cages or free Dox in folate-free RPMI 1640 supplemented with 10% FBS at 37 °C for different times, then fixed with 4% paraformaldehyde and permeabilized with Tris-HCl 0.1 M pH 7.6, Triton 0.1% for 4 min. Biotinylated cages were detected by using streptavidin-FITC (Fluorescein isothiocyanate) (Jackson). For folate receptor detection, membrane immunofluorescence was performed as previously described.[43] Folate receptor was visualized with murine monoclonal antibody (mAb) MOv19[44] as the primary antibody and Rhodamine Red-X-conjugated AffiniPure donkey anti-mouse IgG (Jackson) was used as secondary antibody. The nuclei were stained with DAPI (Invitrogen). Images were obtained with an Olympus FV1000 laser confocal fluorescent microscope at 60x magnification and the fluorescence signal was evaluated with IMARIS software.

Cell Viability Assay

Cell viability was evaluated by using the 3-(4,5-dimethylthiazol-2-yl)-5-(3-carboxymethoxyphenyl)-2-(4-sulfophenyl)-2H-tetrazolium (MTS) assay (Promega). Cells were plated in 96-well plates at a density of 7×10^3/well in RPMI 1640 w/o folic acid supplemented with 2% FBS and incubated for 24 h. After treatment with empty, Dox-loaded Bio-Fol DNA nanocages or free Dox for different times the medium was removed and cells were washed twice in phosphate-buffered saline (PBS). The treatment was refreshed every 24 h incubation. Untreated control groups were incubated with RPMI 1640 w/o folic acid supplemented with 2% FBS. MTS assay was performed at the end of each time of incubation following the manufacturer's instructions. Absorbance was measured at 490 nm using an ELISA plate reader.

Statistical analysis

Data were analysed using Student's "t-test". Results are expressed as a mean ± S.E.M., calculated by using GraphPad Prism. Differences were considered statistically significant when $P < 0.05$ (*) and $P < 0.01$(**).

Results

Modelling and assembly of biotin-folate decorated DNA octahedral cages

The sequences of the oligonucleotides designed for the assembly of DNA truncated octahedral cages having a biotin molecule on one edge of the structure and two folate molecules on another edge are reported in Supplementary Material (Table S1). The presence of folate in the assembled cages allows the binding to the folate receptors and the presence of biotin permits the detection of cages through a streptavidin-biotin reaction. Two folate molecules have been located on a single oligonucleotide (Supplementary Material, Table S1) for maximizing the folate local density and increasing the binding interaction with the receptor.[36] A 3D molecular model for the folate receptor-nanocage complex was built by manually docking the two structures. The model indicates that, using a linker such as triethylene glycol for binding folate to the oligonucleotide, the distance between the folate molecule and the cage is large enough (2.5 nm) for avoiding any steric hindrance between the cage and the folate receptor interacting with the folate molecule. Moreover, as depicted in Figure 1, the close distance between the two folate molecules permits the binding of a single receptor for each cage showing that, once one folate binds to the receptor there is not enough space to permit the binding of the second one to another receptor. The 3D molecular model also shows an

electrostatic complementarity between the strong negative potential surrounding the DNA (red surfaces) and the positive blue potential observed on the face of the receptor interacting with the folate (Figure 1). Following these indications, we have experimentally assembled biotinylated and folate-conjugated (Bio-Fol-) DNA nanocages using oligonucleotides modified by copper(I)-catalysed azide/alkyne cycloaddition (CuAAC, click reaction), as described in Supplementary Material, S2. The assembly of the cages was not perturbed by the presence of the biotin and folate molecules in the oligonucleotides and the assembly efficiency was estimated to be approximately 40%, which is in agreement with previous reports of cage assembly.[6,10,45]

Targeting efficiency of folate-modified DNA nanocages

To evaluate the targeting efficiency of functionalized Bio-Fol-DNA nanocages in living cells we analysed HeLa, HT29, A431 and COS cells known to express the αFR at different levels. HeLa cells were used as αFR overexpressing cell line[33] and A431 cells were used as αFR negative cell lines.[46] Cells were plated at the same density and incubated with 2 μg/ml (3 μM) of Bio-Fol-DNA cages for 24 h at 37°C. After incubation, cells were lysed, centrifuged and supernatants digested with proteinase K for removing the bound proteins that surround the surface of nanocages.[10] DNA nanocages were analysed by DNA blot (Figure 2A). Lanes 1 and 2 show the band of DNA cages (10 and 20 ng respectively) before incubation with the cells (input). DNA cages purified from cell extracts (Figure 2A, lanes 3-6) run mostly as a single product in the gel with mobility comparable to the input, but with a high variability of intensity depending on the cell type analysed. Densitometric analysis allowed us to calculate the amount, expressed in ng/10^6 cells, of DNA cages internalized in 24h in the different cell lines (Figure 2B). The quantity of cages uptaken by HeLa cells was 75±20 ng/10^6 cells, a value more than 40 fold higher than the amount of nanocages internalized into A431 cells (Figure 2A, lanes 4 and 6). The uptake difference is directly correlated to the membrane expression level of αFR receptors as evaluated by flow cytometry (FACS), using two antibodies (MOv19 and MOv18) that recognize different epitopes of the receptor, confirming a good expression of the receptor on the surface of HeLa but not of A431 cells (Supplementary Material, S3). As a further evidence that folate functionalization improve the uptake efficiency of DNA cages in HeLa cells we compared Bio-Fol- with pristine nanocages, finding a 10 fold increase of uptake in the presence of folate (Supplementary Material, S4).

The intracellular localization of Bio-Fol-DNA nanocages was studied by confocal microscopy in HeLa and A431, representing the cell lines with the most and the less efficient cage uptake,

respectively. Cells were stained with streptavidin-FITC for visualizing biotinylated DNA cages and with DAPI for nuclear staining. As shown in Figure 3 (panels A and B), cages appeared in many small fluorescent dots confined in the cytoplasm of HeLa cells whilst no fluorescence was detected in the nuclei. Co-localization analysis using antibodies against the early endosomal antigen (EEA1) for detecting endosomes (Supplementary Material, S5), indicates that endocytic vesicles are involved in the internalization pathway. Notably, DNA cages have a distribution not entirely confined in vesicles likely related to the internalization mechanism of the folate receptors that continuously release folate molecules in the cytoplasm.[32] A431 cells did not show any significant fluorescence signal (panels C and D). The low signal visible in panel C is the same as the fluorescence background of streptavidin-FITC in negative controls (Supplementary Material, S6).

The αFR level in HeLa and A431 cell lines was evaluated using mAb MOv19.[47] In line with the DNA nanocage uptake experiments, shown in Figures 2 and 3 (panels A-D), in HeLa cells αFR receptors are highly expressed as visualized by many plasma membrane associated red fluorescent dots (Figure 3, panels E and F), while A431 cells do not show any red membrane fluorescence around the blue nuclei (Figure 3, panels G and H).

Doxorubicin intercalation to DNA nanocages and drug release in vitro

Dox intercalates into DNA double helix showing a clear selectivity towards GC or CG sequences.[48] At high drug concentration, Dox can also undergo dimerization and form complexes with AT sequences with a lower affinity constant.[42] Octahedral Bio-Fol-DNA nanocages were incubated overnight at RT at different Dox:bp ratio to identify the best loading condition. The unreacted Dox was removed purifying Dox-loaded cages by G25 gel filtration and the Dox leakage was evaluated measuring free Dox fluorescence as a function of time (Supplementary Material, S7), taking advantage of the fluorescence signal of free Dox at 590 nm and of the Dox fluorescence quenching once the drug is intercalated into DNA.[42] The 1:2 Dox:bp ratio resulted to be the best incubation condition leading to a Dox entrapment of 25±4% of the initial concentration with no significant Dox release variation during time (up to 5 days) (Supplementary Material, S7A). These conditions were used for the experiments described from here after.

The *in vitro* pH-dependent Dox release from Dox-loaded octahedral DNA nanocages was quantified through fluorescence spectroscopy, as shown in Figure 4. There was no significant variation of drug release from pH 7.4 to 5.5 while an increase in Dox fluorescence signal was observed at more acidic pH values. The total amount of Dox loaded into DNA cage was evaluated lowering the pH to

2, which causes total Dox release from DNA. It is worth noting that acidifying to pH 2 did not produce any variation to the fluorescence spectra of free Dox (Figure 4B). The time dependent Dox-release profile was further investigated at different pH values (Figure 4C). Purified Dox-loaded DNA nanocages were suspended in TBS pH 7.4, or at pH 5 and 4.5 in citrate buffer 25 mM, NaCl 150 mM (T_0) and fluorescence changes were measured at different time intervals, up to 24 h. At the physiological relevant pH 7.4 Dox-loaded DNA nanocages did not show significant Dox release, while a consistent time-dependent release was observed at pH 4.5, reaching 22% of the total drug concentration after one day.

Dox release was followed as a function of time also in TBS supplemented with 10% FBS (Figure 4D). The presence of 10% FBS slightly increased Dox release after 24 h (about 1%), reaching 8 % after 48 h. The integrity of Dox-loaded DNA nanocages in 10% FBS was tested in parallel by gel electrophoresis as a function of time to verify whether the slight Dox release could be a consequence of degradation of nanocages. Figure 4E shows that DNA cages maintain their integrity for the first 18 hours, while, at longer time, they start to undergo degradation, likely due to the presence of nucleases in FBS.[49] It is worth noting that, after 48 h, a significant amount of nanocages is still intact, as seen by over-exposing the gel (Figure 4E, right panel). In agreement with this finding, incubation of Dox-loaded DNA nanocages with increasing concentration of DNAse I leads to Dox release (Supplementary Material, S8), providing an explanation for the release observed in 10% FBS.

Intracellular trafficking of Dox-loaded DNA cages in HeLa cells

To explore the mechanism of drug delivery, Dox-loaded Bio-Fol-DNA nanocages were incubated with HeLa cells for 4 hours at 37 °C and analysed by confocal microscopy. Dox can be visualized in cells from its own red florescence emission, allowing a direct detection by fluorescence microscopy of the intracellular uptake of Dox molecularly dissolved in the medium (free Dox) or intercalated (Dox-cage), once released from the cages. Cells treated with Dox-cages were stained with streptavidin−FITC for visualizing biotinylated cages (Figure 5). When cells were incubated with free Dox, the drug diffused through cell membranes and it accumulated mostly in cell nuclei (Figure 5A). When doxorubicin was given to cells as Dox-cages it localized in the cytoplasm (Figure 5B-D). Indeed, the confocal images show overlapping red (panel B, Dox) and green (panel C, DNA cages) fluorescence signals, corresponding to co-localization of Dox and DNA cages in the same compartment (panel D, merge). After 4 h incubation, most of the Dox fluorescence signal

(panel B) was still in the cytoplasm, with a low percentage present in the nuclei, indicating that Dox was slowly trafficking to the nuclei.

Dox-loaded DNA nanocage stability in HeLa cells

Empty DNA cages have been shown to be highly stable in biological fluids, in cells and in animal models.[10,50] The effect of Dox intercalation on their *in vitro* stability was investigated as an important prerequisite for their use in biomedical applications. DNA blots demonstrated a slight difference in electrophoretic mobility of Dox-loaded DNA cages when compared with empty DNA cages. After 24 h in culture medium, supplemented with 10% FBS, a low molecular weight smear below the intact Dox-loaded cage band was detectable indicative of partial degradation, in line of what observed for empty cages (Supplementary Material, S9A). We then compared the stability of Dox-loaded or empty DNA nanocages in HeLa cells incubating, for different times, sister cultures with 6 μg/ml (9 μM) of Dox-cages or empty DNA cages at 37 °C. The uptake efficiency and the DNA nanocage integrity were monitored by DNA blot before incubation and after purification from the cells. Lanes 1 and 2 in Figure 6A show 30 ng of empty DNA cages and Dox-cages respectively, in culture medium before incubation with cells (input). DNA cages, purified from cell lysates (lanes 3 and 4) and from conditioned medium (CM) (lanes 5 and 6), derived from both treatment groups, ran as a single product in the gel with mobility comparable to the input, but, in the case of Dox-cages, at much lower intensity (Figure 6A, lanes 4 and 6). From densitometric analysis, the amount of empty DNA cages found in HeLa cells was 317±71 ng/10^6 cells, while that of Dox-cages was 135±29 ng/10^6 cells (compare lane 3 and 4 in Figure 6A). Notably, this latter value is 57±8% lower than the amount of empty DNA cages (Figure 6B). The concentration of DNA cages, purified from CM derived from HeLa cells at the end of the incubation period, was analysed in DNA blot for verifying whether this result was due to lower uptake efficiency or to higher degradation rate of Dox-loaded cages compared to the empty ones. Interestingly, as shown in Figure 6C, also in CM the intensity of the band of Dox-cages was 47±4% lower than the intensity of the band of empty DNA cages (compare lanes 5 and 6, Figure 6A). It is worth noting that free Dox incubated with empty cages in culture medium did not perturb the cage integrity (Supplementary Material, S9B). These findings indicate that the lower amount of Dox-loaded DNA cages found inside HeLa cells is not due to a less efficient internalization of Dox-cages compared to the empty ones but, rather, to their degradation.

Antitumor efficacy of Dox-loaded DNA nanocages

The antitumor efficacy of Dox-loaded Bio-Fol-DNA cages was tested by the MTS assay, incubating for different times Hela and A431 cells with 6 µg/ml (9 µM) and 9 µg/ml (13.5 µM) Dox-cages, containing a loaded Dox concentration of 1.1 and 1.9 µM, respectively, considering that 25% of the initial Dox used for intercalation is present in the Dox-loaded DNA cages (Supplementary Material, S6). Figure 7A shows that the cytotoxic effect obtained in HeLa cells with 6 µg/ml Dox-cages at 48 h, corresponded to 25.7±3% reduction in cell viability. No effect was observed in A431 cells. At 72 hours, a 36±4% reduction over the control was observed (data not shown). Increasing the concentration of Dox-cages to 9 µg/ml, corresponding to 1.9 µM intercalated Dox, the cytotoxic effect was much stronger, leading to 83±3% cell viability reduction at 48 h in HeLa, without producing any effect in A431 cells. Notably, empty DNA nanocages were not cytotoxic at least up to a concentration of 12 µg/ml in both cell types (Figure 7C).

It is worth noting that free Dox, at a concentration of 1.1 µM, did not exert any cytotoxic effect either on HeLa or A431 cells. After 48 h, 2 µM free Dox produced a 25±12% cell viability reduction (Figure 7B), much lower than the 83±3% reduction observed when cells were treated with Dox-loaded DNA nanocages (Figure 7A).

Discussion

In the last years, several attempts to functionalize nanoparticles of different sizes, shapes and materials with ligands of cancer-specific receptors have been reported, with the aim of achieving selective targeting. The results have not always been successful, depending on the ligand accessibility to the receptor. In particular, serum proteins bind and surround the surface of nanoparticles of various origin including DNA nanocages.[10,51,52] This effect, called "*protein corona*" happens in a very short time upon contact with protein-rich biological fluids, in some cases inhibiting the ligand-receptor interaction.[53] We have here demonstrated that the presence of two folate molecules, grafted on the octahedral DNA nanocages at a 2.5 nm distance, allows efficient binding and internalization of cages through a receptor-mediated mechanism into cells overexpressing folate receptors. The presence of the nanocage could even favour the folate-folate receptor interaction due to the presence of a complementary electrostatic potential (Figure 1). Folate receptor-expressing cells internalize DNA cages with an efficiency at least 40 times higher than cells not expressing this receptor (Figure 2). Notably, the alpha isoform of the folate receptor is up-

regulated in many tumours, opening interesting possibilities for exploiting this strategy for cancer treatment.[26]

The here-described DNA-based nanocages have a controllable structure, are easy to assemble and are an efficient binding platform for intercalating drugs, such as doxorubicin. Importantly, we showed that they are highly stable (Figure 2) and not cytotoxic for HeLa cells when incubated without intercalated Dox, up to 48 h (Figure 7C). The loading procedure is easy and Dox release data in solutions of different pH and as a function of time revealed no release at pH 7.4 and a significant increase in release at acidic pH in TBS (Figure 4). The stability of Dox-loaded cages at physiological pH and the pH and time-dependent Dox-release attest to the potential application of DNA nanocages as drug nanocarriers.

When incubated with folate receptor-expressing cells, Dox-loaded Bio-Fol-DNA nanocages were uptaken as efficiently as empty DNA cages and were confined in endocytic vesicles in the cytoplasm, indicating an internalization pathway different from that of free doxorubicin (Figure 5). Free Dox enters into cells by passive diffusion, traffics directly to the nuclei and is quickly metabolized.[22] On the contrary, the receptor-mediated entry of Dox-cages diverts Dox natural traffic slowing its entry to the nuclei.[54] Interestingly, the low pH of endocytic vesicles helps doxorubicin release in the cytoplasm from drug-loaded cages inducing a selective degradation of DNA cages (Figure 6). Dox is known to be a toxic compound that induces several noxious pathways, such as apoptosis and production of reactive oxygen species.[22,23] DNA degradation in cells and in conditioned medium of DNA nanocages (Figure 6) indicates the induction of a DNAse activity, suggesting a caspase-dependent apoptotic mechanism.[55] In this way DNA nanocages not only selectively deliver Dox to the folate receptor-enriched cancer cells, but are also degraded, thus avoiding the problem of nanocarriers accumulation *in vivo*. Another positive finding is that Dox released from the cages is more cytotoxic than free Dox (Figure 7). This result highlights the importance of the different Dox trafficking pathways in triggering cytotoxicity. In the case of Dox-loaded cages, a signalling response at the cytoplasmic level results to be highly cytotoxic.

Taken together these results indicate that functionalization with ligands can be pursued to selectively target DNA nanocages toward cells overexpressing specific receptors, but also demonstrate the need to deeply investigate at the cellular level the pathways induced by the receptor-mediated cell entry to well understand and optimize the killing effect of the drugs.

Acknowledgements

We thank E. Romano from the Centre of Advanced Microscopy "Patrizia Albertano" for skillful assistance in confocal analysis.

References

1 Chen YJ, Groves B, Muscat RA, Seelig G. DNA nanotechnology from the test tube to the cell. *Nat. Nanotechnol*. 2015; **10**:748-760.

2 Krishnan Y, Bathe M. Designer nucleic acids to probe and program the cell. *Trends Cell Biol.* 2012; **22**:624-33.

3 Biocca S, Desideri A. The Potential of Nucleic Acid-Based Nanoparticles for Biomedical Application. *Nano LIFE* 2015; **5**:1541004.

4 Okholm AH, Kjems J. DNA nanovehicles and the biological barriers. *Adv. Drug. Deliv. Rev.* 2016; **106**:183-191.

5 Falconi M, Oteri F, Chillemi G, Andersen FF, Tordrup D, Oliveira CL et al. Deciphering the structural properties that confer stability to a DNA nanocage. *ACS Nano* 2009; **3**:1813-1822.

6 de Oliveira CLP, Juul S, Jørgensen HL, Knudsen B, Tordrup, Oteri F et al. Structure of nanoscale truncated octahedral DNA cages: variation of single-stranded linker regions and influence on assembly yields. *ACS Nano* 2010; **4**:1367-76.

7 Juul S, Iacovelli F, Falconi M, Kragh SL, Christensen B, Frøhlich R et al. Temperature-controlled encapsulation and release of an active enzyme in the cavity of a self-assembled DNA nanocage. *ACS Nano* 2013; **7**:9724-9734.

8 Alves C, Iacovelli F, Falconi M, Cardamone F, Morozzo Della Rocca B, de Oliveira CLP et al. A Simple and Fast Semiautomatic Procedure for the Atomistic Modeling of Complex DNA *Polyhedra. J. Chem. Inf . Model.* 2016, **56**:941-949.

9 Franch O, Iacovelli F, Falconi M, Juul S, Ottaviani A, Benvenuti C et al. DNA hairpins promote temperature controlled cargo encapsulation in a truncated octahedral nanocage structure family. *Nanoscale* 2016; **8**:13333-13341.

10 Vindigni G, Raniolo S, Ottaviani A, Falconi M, Franch O, Knudsen BR et al. Receptor-Mediated Entry of Pristine Octahedral DNA Nanocages in Mammalian Cells. *ACS Nano* 2016; **10**:5971-5979.

11 Jiang Q, Song C, Nangreave J, Liu X, Lin L, Qiu D et al. DNA origami as a carrier for circumvention of drug resistance. *J. Am. Chem. Soc*. 2012; **134**:13396-13403.

12 Li J, Pei H, Zhu B, Liang L, Wei M, He Y, et al. Self-assembled multivalent DNA nanostructures for noninvasive intracellular delivery of immunostimulatory CpG oligonucleotides. *ACS Nano* 2011; **5**:8783-8789;

13 Douglas SM, Bachelet I, Church GM. A logic-gated nanorobot for targeted transport of molecular payloads. *Science* 2012; **335**:831-834.

14 Walsh AS, Yin H, Erben CM, Wood MJ, Turberfield AJ. DNA cage delivery to mammalian cells. *ACS Nano* 2011; **5**:5427-5432.

15 Keum JW, Bermudez H. Enhanced Resistance of DNA Nanostructures to Enzymatic Digestion. *Chem. Commun.* 2009; **45**:7036-7038.

16 Conway JW, McLaughlin CK, Castor KJ, Sleiman H. DNA Nanostructure Serum Stability: Greater than the Sum of Its Parts. *Chem. Commun*. 2013; **49**:1172-1174.

17 Chang M, Yang CS, Huang DM. Aptamer-conjugated DNA icosahedral nanoparticles as a carrier of doxorubicin for cancer therapy. *ACS Nano* 2011; **5**:6156-6163.

18 Kim KR, Kim DR, Lee T, Yhee JY, Kim BS, Kwon IC et al. Drug delivery by a self-assembled DNA tetrahedron for overcoming drug resistance in breast cancer cells. *Chem. Commun*. 2013; **49**:2010-2012.

19 Kumar V, Bayda S, Hadla M, Caligiuri I, Russo Spena C, Palazzolo S et al. Enhanced Chemotherapeutic Behavior of Open-Caged DNA@Doxorubicin Nanostructures for Cancer Cells. *J. Cell. Physiol*. 2016; **231**:106-110.

20 Setyawati MI, Kutty RV, Leong DT. DNA Nanostructures Carrying Stoichiometrically Definable Antibodies. *Small* 2016; **12**:5601-5611.

21 Cortés-Funes H, Coronado C. Role of anthracyclines in the era of targeted therapy. *Cardiovasc. Toxicol*. 2007; **7**:56-60.

22 Minotti G, Menna P, Salvatorelli E, Cairo G, Gianni L. Anthracyclines: molecular advances and pharmacologic developments in antitumor activity and cardiotoxicity. *Pharmacol. Rev.* 2004; **56**:185-229.

23 Yang F, Teves SS, Kemp CJ, Henikoff S. Doxorubicin, DNA torsion, and chromatin dynamics. *Biochim. Biophys. Acta* 2014; **1845**: 84–89.

24 Gewirtz DA. A critical evaluation of the mechanisms of action proposed for the antitumor effects of the anthracycline antibiotics adriamycin and daunorubicin. *Biochem. Pharmacol*. 1999; **57**:727-741.

25 Meredith AM, Dass CR. Increasing role of the cancer chemotherapeutic doxorubicin in cellular metabolism. *J. Pharm. Pharmacol*. 2016; **68**:729-741.

26 Zwicke GL, Mansoori GA and Jeffery CJ. Utilizing the folate receptor for active targeting of cancer nanotherapeutics. *Nano Rev*. 2012; **3**, DOI: 10.3402/nano.v3i0.18496.

27 Despierre E, Lambrechts S, Leunen K, Berteloot P, Neven P, Amant F et al. Folate receptor alpha (αFR) expression remains unchanged in epithelial ovarian and endometrial cancer after chemotherapy. *Gynecol. Oncol*. 2013; **130**:192-199.

28 Crane LM, Arts HJ, van Oosten M, Low PS, van der Zee AG, van Dam GM et al. The effect of chemotherapy on expression of folate receptor-alpha in ovarian cancer. *Cell Oncol*. 2012, **35**:9-18.

29 Parker N, Turk MJ, Westrick E, Lewis JD, Low PS, Leamon CP. Folate receptor expression in carcinomas and normal tissues determined by a quantitative radioligand binding assay. *Anal. Biochem*. 2005; **338**:284-293.

30 Paulos CM, Reddy JA, Leamon CP, Turk MJ, Low PS. Ligand binding and kinetics of folate receptor recycling in vivo: impact on receptor-mediated drug delivery. *Mol. Pharmacol*. 2004; **66**:1406-1414.

31 Chen C, Ke J, Zhou XE, Yi W, Brunzelle JS, Li J et al. Structural basis for molecular recognition of folic acid by folate receptors. *Nature* 2013; **500**:486-489.

32 Wang S, Low PS. Folate-mediated targeting of antineoplastic drugs, imaging agents, and nucleic acids to cancer cells. *J. Control Release* 1998; **53**:39-48.

33 Cheung A, Bax HJ, Josephs DH, Ilieva KM, Pellizzari G, Opzoomer J et al. Targeting folate receptor alpha for cancer treatment. *Oncotarge*t 2016; **7**:52553-52574.

34 Kocabey S, Meinl H, MacPherson IS, Cassinelli V, Manetto A, Rothenfusser S et al. Cellular Uptake of Tile-Assembled DNA Nanotubes. *Nanomaterials* 2015; **5**:47-60.

35 Ko S, Liu H, Chen Y, Mao C. DNA nanotubes as combinatorial vehicles for cellular delivery. *Biomacromolecules* 2008; **9**:3039-3043.

36 Lee H, Lytton-Jean AK, Chen Y, Love KT, Park AI, Karagiannis ED et al. Molecularly selfassembled nucleic acid nanoparticles for targeted in vivo siRNA delivery. *Nat. Nanotechnol*. 2012; **7**:389-393.

37 Gramlich PM, Wirges CT, Manetto A, Carell T. Postsynthetic DNA modification through the copper-catalyzed azide-alkyne cycloaddition reaction. *Angew. Chem. Int. Ed. Engl*. 2008; **47**:8350-8358.

38 Bernstein FC, Koetzle TF, Williams GJB, Meyer EF, Brice MD, Rodgers JR et al. The Protein Data Bank: A Computer-Based Archival File for Macromolecular Structures. *Arch. Biochem. Biophys*. 1978; **185**:584-591.

39 Kim S, Thiessen PA, Bolton EE, Chen J, Fu G, Gindulyte A et al. PubChem Substance and Compound Databases. *Nucleic Acids Res*. 2016; **44**:D1202-D1213.

40 Dolinsky TJ, Nielsen JE, McCammon JA, Baker NA. PDB2PQR: An Automated Pipeline for the Setup of Poisson-Boltzmann Electrostatics Calculations. *Nucleic Acids Res.* 2004; **32**:W665-W667.

41 Baker NA, Sept D, Joseph S, Holst MJ, McCammon JA. Electrostatics of Nanosystems: Application to Microtubules and the Ribosome. *Proc. Natl. Acad. Sci*. 2001; **98**:10037-10041.

42 Pérez-Arnaiz C, Busto N, Leal JM, García B. New insights into the mechanism of the DNA/doxorubicin interaction. *J Phys Chem B*. 2014; **118**:1288-95.

43 Cardinale A, Filesi I, Vetrugno V, Pocchiari M, Sy MS, Biocca S. Trapping prion protein in the endoplasmic reticulum impairs PrP^{C} maturation and prevents PrP^{Sc} accumulation. *J. Biol. Chem.* 2005; **280**:685-694.

44 Miotti S, Canevari S, Ménard S, Mezzanzanica D, Porro G, Pupa SM et al. Characterization of human ovarian carcinoma-associated antigens defined by novel monoclonal antibodies with tumor-restricted specificity. *Int. J. Cancer* 1987; **39**:297-303.

45 Andersen FF, Knudsen B, Oliveira CL, Frøhlich RF, Krüger D, Bungert J et al. Assembly and structural analysis of a covalently closed nanoscale DNA cage. *Nucleic Acids Res*. 2008; **36**:1113-1119.

46 Bagnoli M, Tomassetti A, Figini M, Flati S, Dolo V, Canevari S et al. Downmodulation of caveolin-1 expression in human ovarian carcinoma is directly related to alpha-folate receptor overexpression. *Oncogene* 2000; **19**:4754-4763.

47 Coney LR, Tomassetti A, Carayannopoulos L, Frasca V, Kamen BA, Colnaghi MI et al. Cloning of a tumor-associated antigen: MOv18 and MOv19 antibodies recognize a folate-binding protein. *Cancer Res.* 1991; **51**:6125-6132.

48 Ren J, Chaires JB Sequence and structural selectivity of nucleic acid binding ligands. *Biochemistry* 1999; 38:16067-75

49 von Köckritz-Blickwede M, Chow OA, Nizet V. Fetal calf serum contains heat-stable nucleases that degrade neutrophil extracellular traps. *Blood* 2009; **114**:5245-6

50 Surana S, Bhatia D, Krishnan Y. A method to study in vivo stability of DNA nanostructures. *Methods* 2013; **64**:94-100.

51 Tenzer S, Docter D, Kuharev J, Musyanovych A, Fetz V, Hecht R et al. Rapid Formation of Plasma Protein Corona Critically Affects Nanoparticle Pathophysiology. *Nat. Nanotechnol.* 2013; **10**:772-781.

52 Pelaz B, del Pino P, Maffre P, Hartmann R, Gallego M, Rivera-Fernández S et al. Surface Functionalization of Nanoparticles with Polyethylene Glycol: Effects on Protein Adsorption and Cellular Uptake. *ACS Nano* 2015; **9**:6996-7008.

53 Salvati A, Pitek AS, Monopoli MP, Prapainop K, Bombelli FB, Hristov DR et al. Transferrin-functionalized nanoparticles lose their targeting capabilities when a biomolecule corona adsorbs on the surface. *Nat. Nanotechnol*. 2013; **8**:137-143.

54 Halley P, Lucas CR, McWilliams EM, Webber MJ, Patton RA, Kural C et al. Daunorubicin-Loaded DNA Origami Nanostructures Circumvent Drug Resistance Mechanisms in a Leukemia Model. *Small* 2016; **12**:308-320.

55 Enari M, Sakahira H, Yokoyama H, Okawa K, Iwamatsu A, Nagata S. A caspase-activated DNase that degrades DNA during apoptosis, and its inhibitor ICAD. *Nature* 1998; **391**:43-50.

Legends to Figures

Figure 1. Electrostatic potential distribution around the Bio-Fol-DNA nanocage-folate receptor complex. (A) View of the full complex. (B) Close view of the folate protruding from the cage bound to the receptor. Negative and positive electrostatic potentials are represented by red and blue colours respectively.

Figure 2. Folate receptor-mediated uptake of Bio-Fol-DNA nanocages in cells. (A) Representative DNA blotting of cell extracts obtained from COS (lane 3), HeLa (lane 4), HT29 (lane 5) and A431 (lane 6) cells. DNA cages were detected with streptavidin-HRP. Purified DNA nanocages before incubation with cells (input) are shown in lanes 1 (10 ng) and 2 (20 ng). (B) Histogram shows the calculated amount of DNA nanocages internalized in different cell lines, as indicated. Values were expressed as a mean ± SEM.

Figure 3. Confocal analysis of Bio-Fol-DNA cages internalized in HeLa and A431 cells. (A-D) Biotinylated cages are detected using streptavidin-FITC and nuclei are blue stained with DAPI. (E-H) Confocal analysis of folate receptor expression analysed with monoclonal antibody MOv19. αFR receptors are visualized in red, nuclei are blue stained with DAPI. Scale bar: 20 μm.

Figure 4. *In vitro* release of Dox from Dox-loaded DNA nanocages. (A) Fluorescence spectra of released Dox at different pH. (B) Fluorescence spectra of free Dox at pH 7.4 and 2.0. (C) Percentage of time-dependent Dox release from Dox-loaded cages at pH 7.4, 5 and 4.5, monitored by fluorescence changes (Excitation: 485 nm; Emission: 590 nm). (D) Percentage of Dox release from Dox-loaded cages in the presence of 10% FBS, monitored by fluorescence changes and (E) DNA blot of Dox-loaded DNA nanocages in the presence of 10% FBS at different times. The right panel shows a 5x exposure of the lane corresponding to the 48 h sample.

Figure 5. Intracellular distribution of Dox. Hela cells were treated with 2.5 μM free Dox (panel A) or 13 μg/ml Dox-loaded cages (panels B-D) for 4 h. Biotinylated cages are detected using streptavidin-FITC and nuclei are blue stained with DAPI. Scale bar: 20 μm.

Figure 6. Stability of Dox-loaded cages in lysates of HeLa cells and in conditioned medium (CM). (A) Representative DNA blotting of cell lysates and CM obtained from cells incubated for 4 h with empty (lanes 3 and 5) and Dox-loaded (lanes 4 and 6) Bio-Fol-DNA cages. Lane 1 (empty cages) and lane 2 (Dox-loaded cages) show 30 ng of DNA nanocages before incubation with cells (input). (B) Percentage of empty and Dox-loaded DNA nanocages detected in cell lysates. (C) Percentage of empty and Dox-loaded DNA nanocages detected in CM. Histograms show the densitometric analysis of three different experiments.

Figure 7. Cell viability of Hela and A431 cells treated with (A) Dox-loaded cages, (B) free Dox and (C) empty cages at increasing concentrations and times, as indicated. Rectangles in (B) indicate the amount of Dox intercalated in the Dox-cages used for the experiments shown in A and rectangles in (C) indicate the amount of empty cages used for the experiments shown in A. The data represent the mean ±S.E.M. of three separate experiments. $P < 0.05$ (*) and $P < 0.01$(**).

Figure 1

Click here to download high resolution image

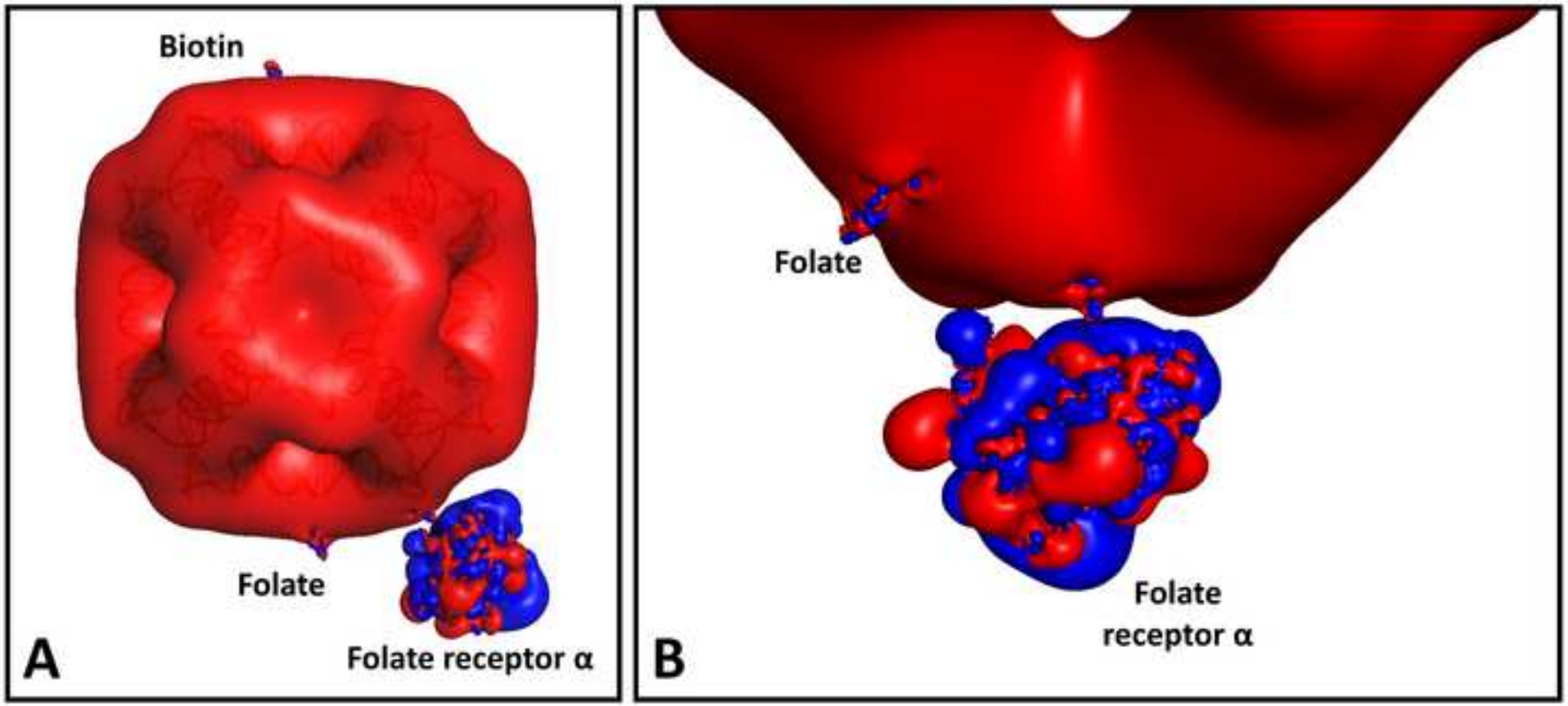

Figure 2

Click here to download high resolution image

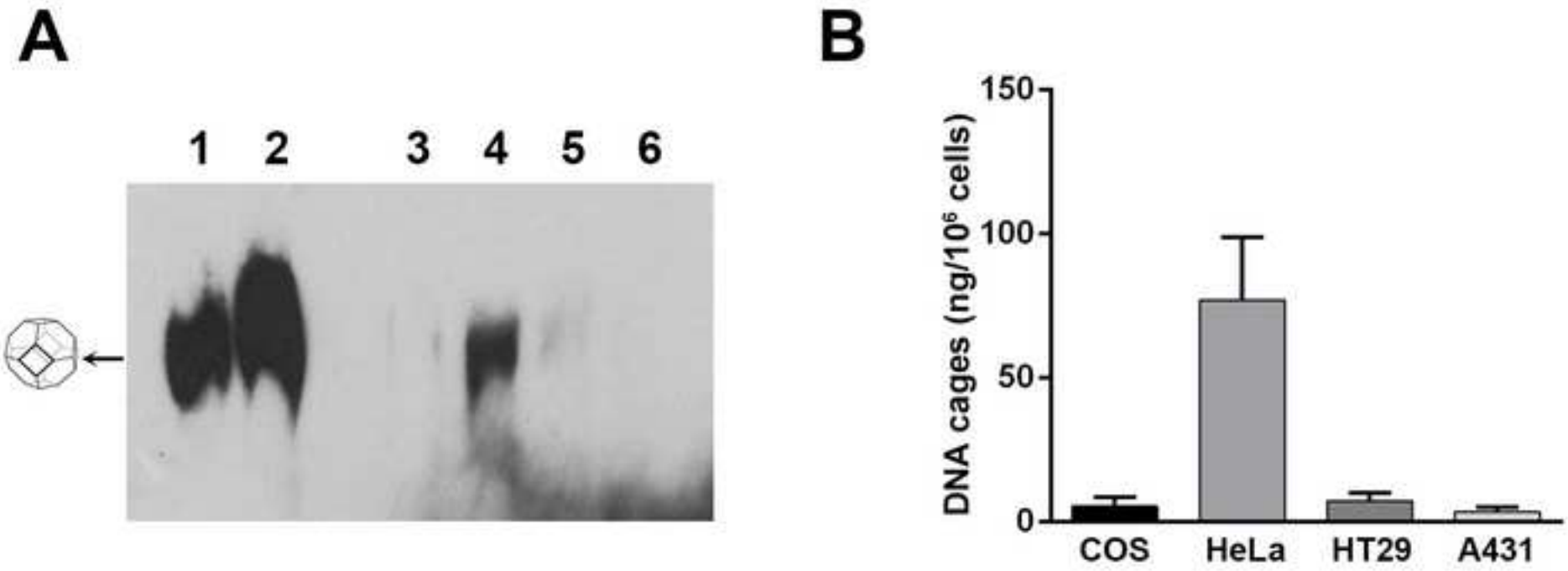

Figure 3

Click here to download high resolution image

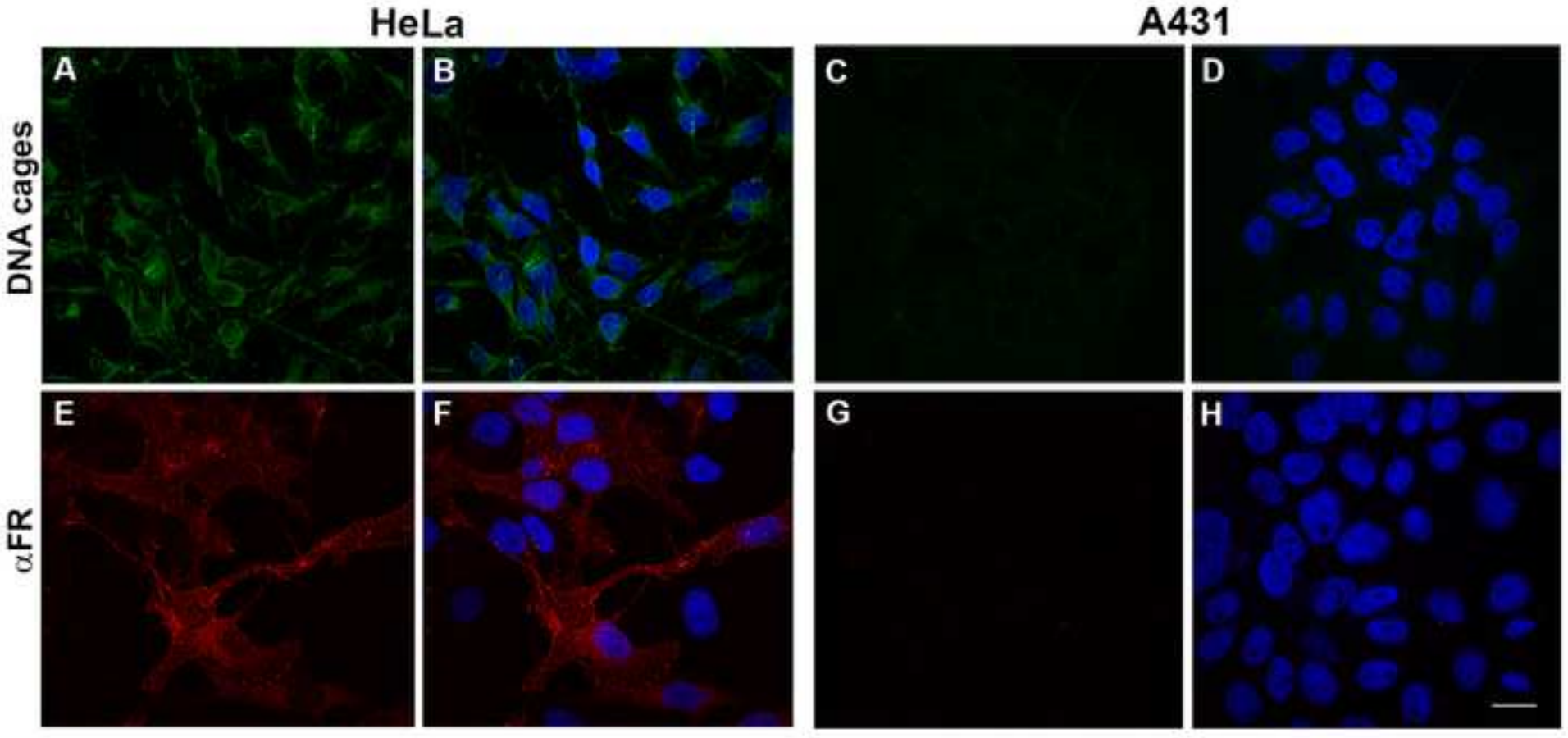

Figure 4

Click here to download high resolution image

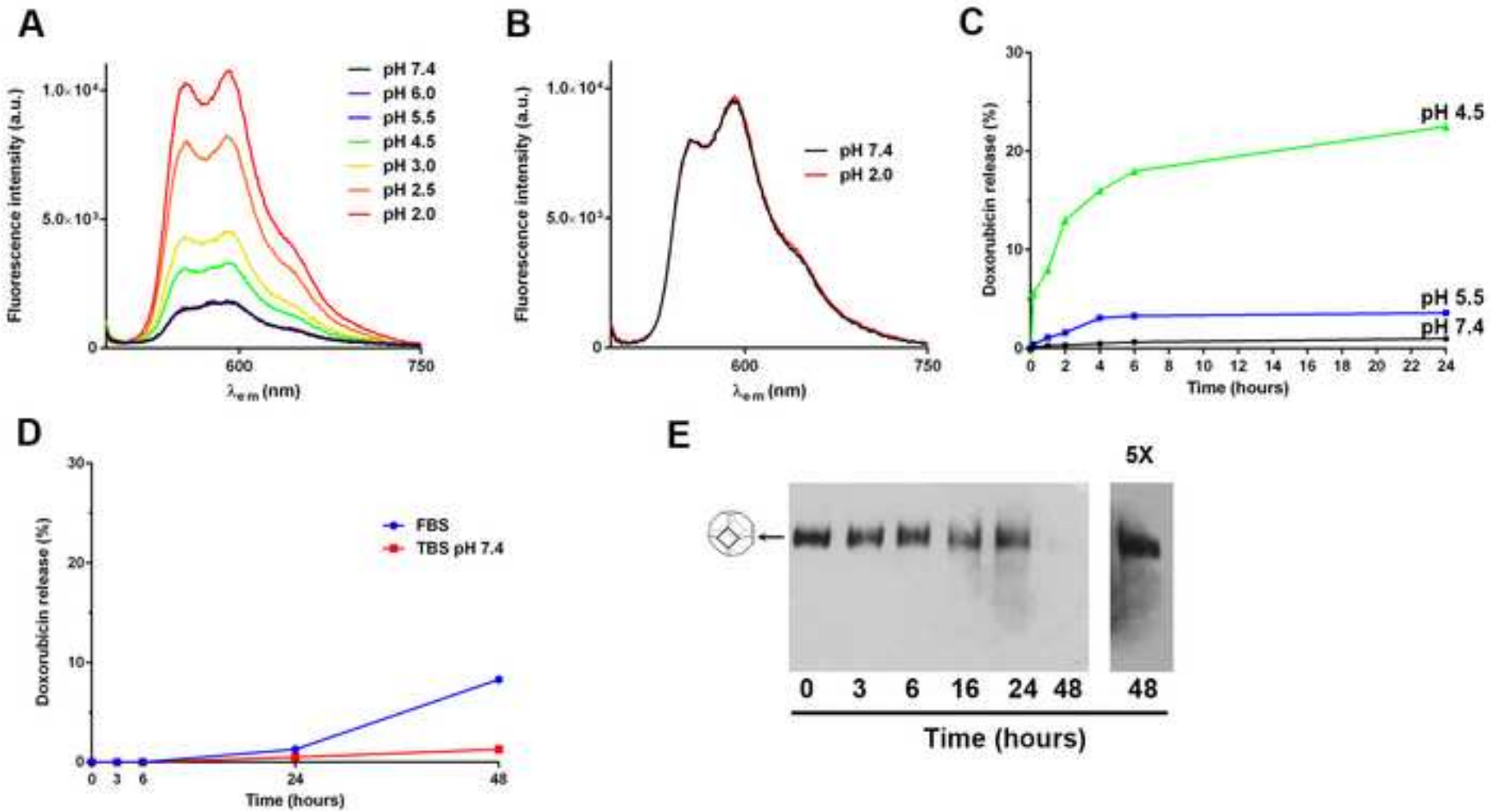

Figure 5

Click here to download high resolution image

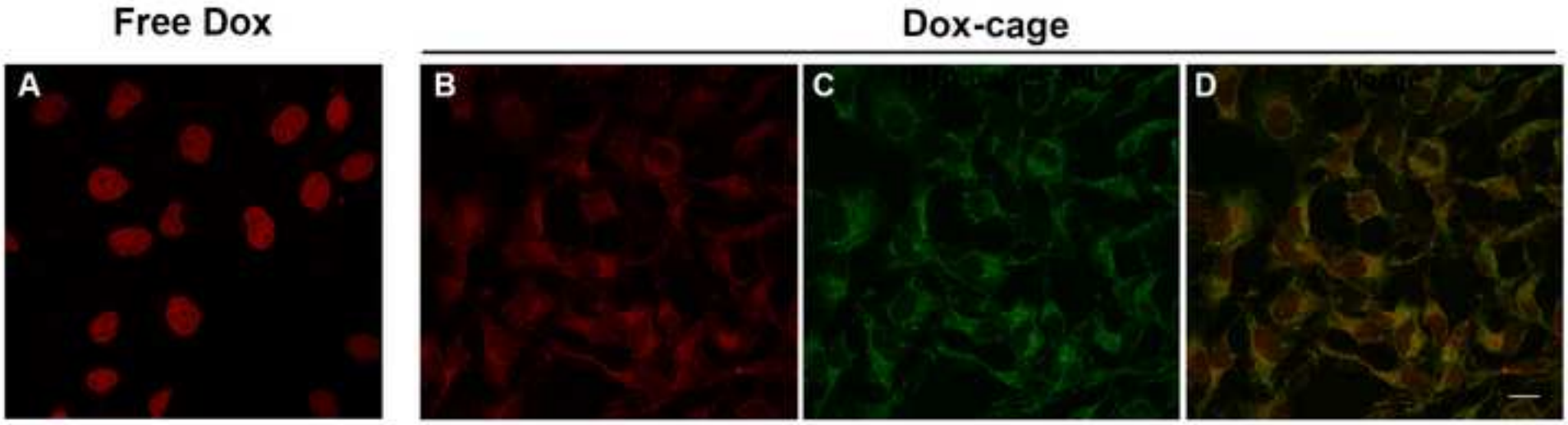

Figure 6

Click here to download high resolution image

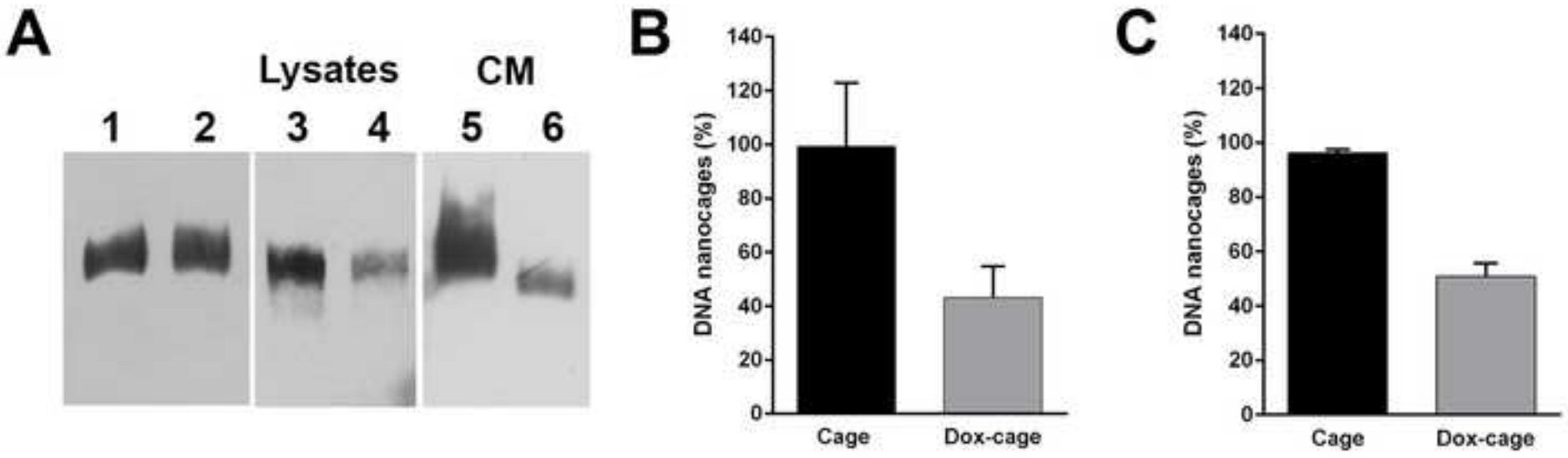

Figure 7

Click here to download high resolution image